



Structural formation during bread baking in a combined microwave-convective oven determined by sub-second in-situ synchrotron

Downloaded from: <https://research.chalmers.se>, 2025-12-04 17:52 UTC

Citation for the original published paper (version of record):

Schott, F., Isaksson, S., Larsson, E. et al (2023). Structural formation during bread baking in a combined microwave-convective oven determined by sub-second in-situ synchrotron X-ray microtomography. Food Research International, 173. <http://dx.doi.org/10.1016/j.foodres.2023.113283>

N.B. When citing this work, cite the original published paper.



Structural formation during bread baking in a combined microwave-convective oven determined by sub-second in-situ synchrotron X-ray microtomography

Florian Schott^{a,*}, Sven Isaksson^b, Emanuel Larsson^{a,b}, Federica Marone^c, Camilla Öhgren^b, Magnus Röding^{b,d}, Stephen Hall^a, Niklas Lorén^{b,e,*}, Rajmund Mokso^{f,a}, Birgitta Wäppling Raaholt^b

^a Division of Solid Mechanics, Faculty of Engineering, Lund University, Lund, Sweden

^b Department of Agriculture and Food, Research Institutes of Sweden (RISE), 402 29 Göteborg, Sweden

^c Swiss Light Source, Paul Scherrer Institute, 5232 Villigen, Aargau, Switzerland

^d Department of Mathematical Sciences, Chalmers University of Technology and University of Gothenburg, Göteborg, Sweden

^e Department of Physics, Chalmers University of Technology, 41296 Göteborg, Sweden

^f Department of Physics, Technical University of Denmark, DK-2800 Kgs. Lyngby, Denmark

ARTICLE INFO

Keywords:

Bread
Baking
Microwave
Convective
Oven
Synchrotron X-ray microtomography
In-situ
Image analysis

ABSTRACT

A new concept has been developed for characterizing the real-time evolution of the three-dimensional pore and lamella microstructure of bread during baking using synchrotron X-ray microtomography (SRμCT). A commercial, combined microwave-convective oven was modified and installed at the TOMCAT synchrotron tomography beamline at the Swiss Light Source (SLS), to capture the 3D dough-to-bread structural development *in-situ* at the micrometer scale with an acquisition time of 400 ms. This allowed characterization and quantitative comparison of three baking technologies: (1) convective heating, (2) microwave heating, and (3) a combination of convective and microwave heating. A workflow for automatic batchwise image processing and analysis of 3D bread structures (1530 analyzed volumes in total) was established for porosity, individual pore volume, elongation, coordination number and local wall thickness, which allowed for evaluation of the impact of baking technology on the bread structure evolution. The results showed that the porosity, mean pore volume and mean coordination number increase with time and that the mean local cell wall thickness decreases with time. Small and more isolated pores are connecting with larger and already more connected pores as function of time. Clear dependencies are established during the whole baking process between the mean pore volume and porosity, and between the mean local wall thickness and the mean coordination number. This technique opens new opportunities for understanding the mechanisms governing the structural changes during baking and discern the parameters controlling the final bread quality.

1. Introduction

White bread is an essential part of the diet and gastronomic culture globally. The food industry has an interest in better understanding the impact of the baking processes on the final bread quality, aiming for a better use of resources (time, energy, and raw materials). Baking is still an energy intensive process, and microwave baking has a great potential for making it more energy efficient, potentially down to approximately

25–33% of the convective baking energy consumption (Wäppling Raaholt et al, 2011, Wäppling-Raaholt, 2013, 2015, 2020). Microwave technology is today mainly used when crust formation is not necessary, such as for baking crustless bread and sponge cakes with icing. However, microwave-convective baking is an interesting alternative that combines the advantage from both technologies; namely, the crust formation and the flavor development, while an improved baking time and energy performance. Additional work is currently required to better understand

Abbreviations: RISE, Research Institutes of Sweden; SRμCT, synchrotron X-ray microtomography; SLS, Swiss Light Source; μCT, microtomography; PEEK, polyetheretherketone; VOI, volume-of-interest.

* Corresponding authors.

E-mail addresses: florian.schott@solid.lth.se (F. Schott), niklas.loren@ri.se (N. Lorén).

<https://doi.org/10.1016/j.foodres.2023.113283>

Received 29 March 2023; Received in revised form 12 July 2023; Accepted 13 July 2023

Available online 17 July 2023

0963-9969/© 2023 The Author(s). Published by Elsevier Ltd. This is an open access article under the CC BY license (<http://creativecommons.org/licenses/by/4.0/>).

Table 1

Experimental design includes the baking technologies and their relevant parameters, flour types, and vertical positions of the volume-of-interest (VOI) from the sample holder.

Baking technology			Bread flour			Volume-of-interest	
	T (°C)	Microwave power (W)	Baking time (min)		Protein content		Position Z (cm)
Convective	220	0	11	Spring wheat	13.3	wt%	Bottom
Microwave	30	300	2	Kondis	9.5	wt%	Middle
Combined	230	100	5	Extra	13.3	wt%	Top

the influence of the baking process on the resulting bread quality and especially on its cellular microstructure. The overall aim of this work was to demonstrate a new concept to follow the *in situ* structure evolution during baking and to inspire the increased use of synchrotron x-ray microtomography in food science. The detailed aims of this work were to (i) develop a combined microwave/convection that can be used for synchrotron x-ray microtomography measurements (SRμCT), (ii) perform *in situ* imaging of the 3D structure evolution during baking using SRμCT; (iii) develop a workflow for efficient segmentation and image analysis of the obtained 3D data; (iv) investigate the effect of baking process (convection, combined, microwave), protein content and imaging position on the bread structure evolution.

Bread-baking is a complex process, due to the combination of heat induced structural changes and chemical processes, such as expansion of the pores, formation of crumb and crust, inactivation of yeast, and flavor development (Mondal & Datta, 2008; Chhanwal, Tank, Raghavarao, & Anandharamakrishnan, 2012; Briceño-Ahumada, Mikhailovskaya, & Staton, 2022). *In situ* time-resolved bread structure analysis is challenging since baking occurs inside an oven and in the bread bulk. Most of the previous studies on bread baking have been done stepwise, with different samples being extracted at different times and at various baked states. This results in many analyzed samples, and provides information about the average structure evolution (Sluimer, 2005; Primo-Martín et al., 2010). The main limitations of that method are the interruption of the baking process, inducing interferences with the pore structure formation, and the impossibility to follow the changes in a unique sample during the entire baking process. X-ray microtomography (μCT) is today a well-established technique for studies on the microstructure of cellular food products (Falcone et al., 2006a) such as porous bread (Falcone et al., 2006b; Lassoued et al., 2007). It is a non-destructive imaging technique, does not require additional sample preparation, is optimal for scanning low-absorbing samples, and allows to quantitatively describe the morphology of the microstructure (Laverse, Frisullo, Conte, & Nobile, 2012). Recent advances in synchrotron X-ray microtomography (SRμCT) makes it possible to study the gas-pore nucleation and their evolution inside a bread during baking. Thanks to the high photon flux offered by synchrotron sources, Babin et al. (2006) recorded in-situ bread baking inside a standard convective oven. A full tomography was recorded in 30 s. SRμCT has also been used to investigate the effect of salt on the bubble structure evolution in wheat flour doughs (Sun et al., 2020). A full tomography was recorded in either 74 s or 120 s depending on the used beamline. While these time resolutions were sufficient for studying proofing or convective bread baking, a faster image acquisition is required to follow and quantify the structure evolution of bread during microwave baking due to much faster structural changes. Furthermore, in-situ imaging with microwave baking is additionally challenging regarding microwave leakage.

The presented concept shows strong potential in using SRμCT imaging for quantitative determination of the influence of baking technology on the bread structure evolution and the final bread quality. The quantitative measures determined from the bread pore and lamella structures over time, include parameters such as, porosity, pore volume, coordination, elongation and lamella thickness, partly similar to the work from Laverse et al. (2012). The protein content plays a concomitant role with the baking technology in determining the bread quality.

The desired soft crumb and crisp crust in white bread are directly influenced by the cellular structure morphology (Primo-Martín et al., 2010) and the structural key element for wheat flour is the protein content (Hu et al., 2021; Johansson et al., 2002; Sluimer, 2005). For example, low protein content flour typically yields a dough with high gas permeability resulting in a bread with low rise volume and poor internal crumb structure (Chamberlain, 1973). However, the interplay between the baking process and the formulation on the baking quality are still not fully understood.

In this work, the bread structure evolution was successively assessed and quantified during combined microwave-convective baking by modifying a commercial oven and using *in-situ* 3D X-ray imaging at both a high spatial resolution (11 μm voxel size) and time resolution (400 ms full tomographic acquisition) with the fast-scanning abilities at the TOMCAT beamline at the Swiss Light Source, Paul Scherrer Institute. The image reconstruction was followed by an image quantification protocol, that allowed for determination of porosity, local wall thickness, pore volume, elongation, and pore coordination number. The capabilities of the concept are demonstrated by comparing three baking technologies: microwave baking (*Microwave*), convective baking (*Convective*), and microwave-convective baking (*Combined*) at three different positions inside the dough items. Data was also collected for two flour varieties: naturally high gluten (*Spring wheat*), naturally low gluten (*Kondis*) and *Kondis* with added gluten (*Extra*) to relate both to the protein concentration and flour force. The presentation of results is primarily based on the *Extra* flour. Two general observed correlations for all the samples are also presented at the end of this work.

2. Methods

2.1. Oven compatibility with synchrotron X-ray microtomography

Combined microwave-convective baking as imaged by SRμCT at the TOMCAT beamline (Paul Scherrer Institute, Swiss Light Source, Switzerland) was successfully done by modifying a commercial oven (Electrolux OOM1000CZ) at RISE. The modified oven was assembled at RISE and implemented at TOMCAT, and the modifications are shown in the appendix A in Fig. A.1. Two aluminum windows (0.5 mm thick sheets) were installed on both sides of the oven, allowing X-ray transmission, while encapsulating the microwaves. These windows were attached with high-temperature resistant aluminum tape. The oven walls were originally stamping-pressed. Since the position and geometry of these partly coincided with the desired position of the aluminum windows, the introduction of the latter resulted in some changes also of the stamping-pressed geometry. Tomographic imaging requires the bread samples to rotate around a vertical axis inside the oven. This was achieved by placing the bread on a custom-made sample holder. The sample holder was made of polyetheretherketone (PEEK) plastic which provides good thermal stability and X-ray transparency. An 8 mm-diameter hole was drilled at the bottom of the oven to accommodate the sample holder shaft and enable connection to the beamline rotate stage. The plastic shaft was extended at the bottom by a 28 mm metallic cylinder to suppress microwave leakage due to evanescent modes. The lower part of the sample holder shaft outside the oven was additionally air-cooled by continuous room temperature pressurized air flow. More

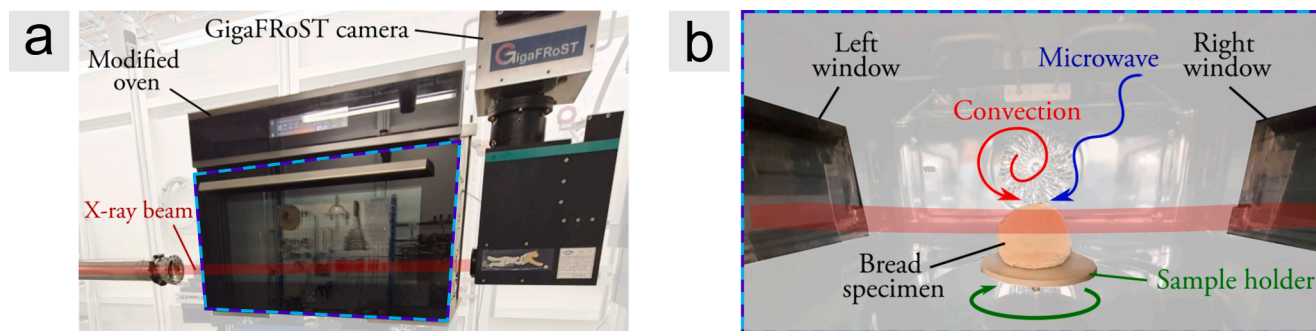


Fig. 1. (a) The oven-tomography setup at TOMCAT. The X-ray beam (in red) propagates through the modified oven and are collected by the GigaFROST CMOS camera after exiting the oven. The oven chamber is highlighted by a dashed cyan-blue box. (b) Inside view of the modified oven chamber, showing the two aluminum windows (the X-ray entering from the left and outgoing on the right) and a bread sample on the sample holder. The X-ray radiographies of the bread can be acquired while being simultaneously baked by convection and microwave heating. (For interpretation of the references to color in this figure legend, the reader is referred to the web version of this article.)

details on these modifications are shown in the appendix A.

2.2. Experimental design

The experimental design involved three different parameters: (1) baking technology, (2) flour type and (3) vertical position inside the breads. For baking technology, the effect of microwave baking (*Microwave*), convective baking (*Convective*), and microwave-convective baking (*Combined*), on the bread structure evolution was evaluated. The variations in flour type included naturally high gluten (*Spring wheat*), naturally low gluten (*Kondis*) and artificially high gluten (*Extra*). The effect the bottom (*Bottom*), middle (*Middle*) and top (*Top*) positions inside the buns, on the structure evolution was also evaluated. During each experiment the position of the sample stage was fixed and a specific volume inside the bread buns was not followed due to the highly not linear evolution of the bread microstructure, not known a priori. Table 1 summarizes the 27 different cases in the experimental design.

The three flours were prepared from two different wheat flours, one flour with a naturally high protein-content, called *Spring wheat*, and one flour with a naturally low protein-content, called *Kondis* (official brand name of Abdon Food AB, Helsingborg, Sweden). Their protein contents were 13.3 wt% and 9.5, respectively, with a standard deviation of 0.003 wt%. The measures were done in duplicates from the total nitrogen content, according to the Dumas combustion method (Saint-Denis & Goupy, 2004) and using a LECO TruMac nitrogen analyzer

(LECO Corporation, USA). A nitrogen-to-protein conversion factor of 5.7 was used for calculating the protein content, in accordance with ISO/TS 16634-2:2009 for wheat flour (Müller, 2017). The *Kondis* and *Spring wheat* doughs were based solely on *Kondis* and *Spring wheat* flour, respectively. However, *Extra* dough was instead prepared by strengthening the *Kondis* flour with artificially added gluten (Manildra Milling Corp., 72.0 ± 0.7 wt% protein) to reach the same protein content as the *Spring wheat* dough. The rest of the recipe was similar for the three dough types (Thorén, 2020): 1110 g flour (pure or with added gluten), 18 g salt, 18 g sugar, 18 g rapeseed oil, 600 g water and 13.5 g dry yeast. The ingredients were mixed in a laboratory kneader (VMI Linix group, SPI-LAB, Saint-Hilaire-de-Loulay, France) for 2 min at low speed (dough hook rotating at 60 rpm, bowl rotating at 6 rpm) and for 7 min at high speed (dough hook rotating at 180 rpm, bowl rotating at 15 rpm). The temperature of the doughs after mixing was estimated to 22–25 °C based on previous experience using the same dough kneader. After kneading, the dough was left to rest for 10 min, and then rolled into buns weighing (90.0 ± 0.5) g. The resulting dough items were put in a freeze room equipped with forced air circulation at -40 °C, and then sent to TOMCAT in thermally insulated boxes three weeks after their production, and two days prior to the experiment. The dough items were inspected upon arrival, and those showing signs of thawing were discarded, whereas intact items were placed in a freezer at -18 °C. One by one, they were finally defrosted and proofed in a laboratory oven (Thermo Scientific Heraeus, U.S.) at 40 °C for 120 min before baking. The dough items were

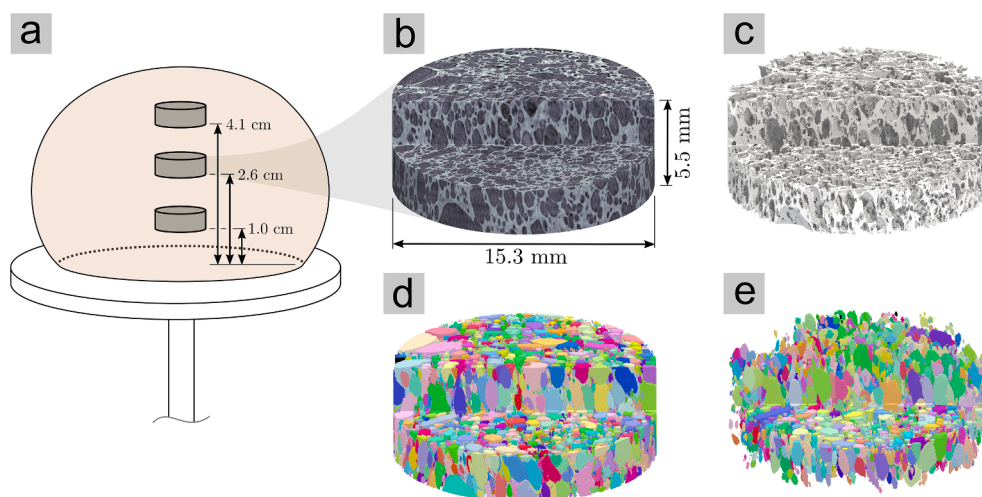


Fig. 2. (a) Diagram showing the extracted volume-of-interest (VOI) inside the breads, i.e. bottom, middle and top positions. (b–e) post-processing steps for the first image from the *Extra-Middle-Convective* series ($t = 6.4$ s): (b) reconstructed image, (c) segmented image, (d) separated pores and (e) separated pores with removed pores at the edges, top and bottom. The pores are labelled with arbitrary colors.

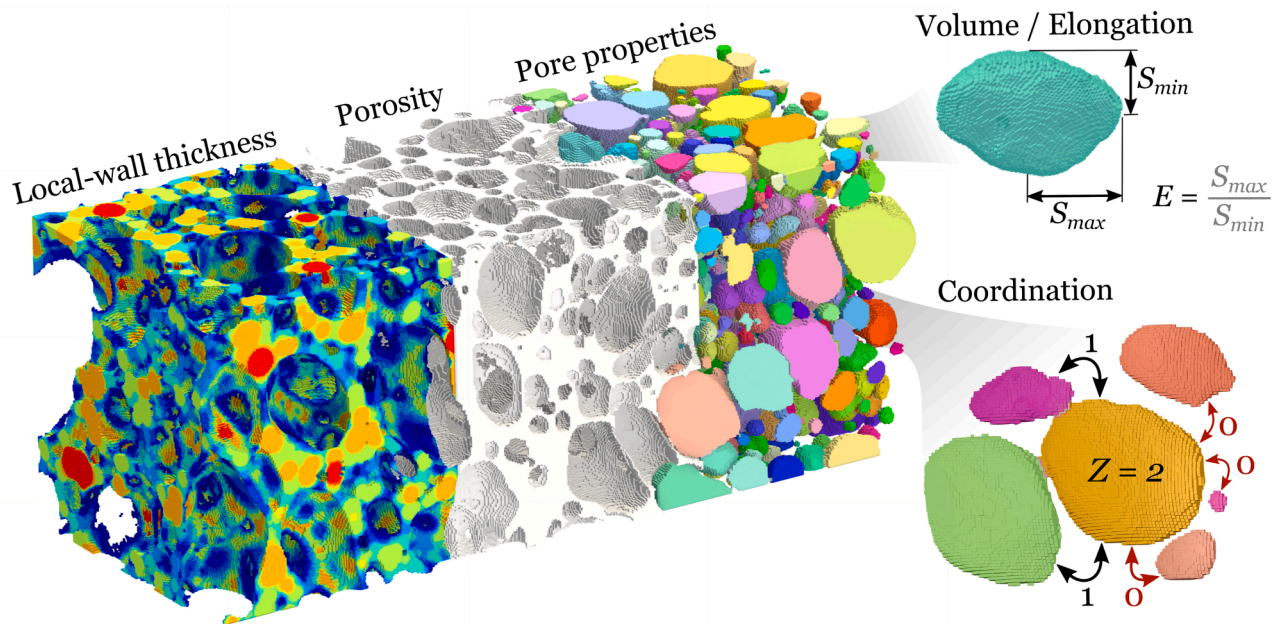


Fig. 3. Diagram showing the extracted bread property: from the left to the right, the local-wall thickness h_w , the porosity ϕ_g , the individual pore volume V , elongation E , and coordination number Z . The larger local-wall thicknesses regions are shown in red and the smaller ones in dark blue. The pores are labelled with arbitrary colors. The ratio of the maximum shape eigenvalue by the minimum shape eigenvalue gives the elongation E of the cyan pore. The coordination of the mustard pore is equal to two, by its contact with the purple and the green pore regions (on the left). However, it is not in contact with the orange, salmon and pink pores (on the right). (For interpretation of the references to color in this figure legend, the reader is referred to the web version of this article.)

sprayed with water every 20 min to maintain a moist surface (3 sprays per occasion). A water container was additionally placed inside the proving oven to ensure a high ambient humidity.

Baking was either purely convective for 11 min at 220 °C (*Convective*), purely with microwave for 2 min at 300 W power and at room temperature (*Microwave*) or combined convective-microwave for 5 min at 230 °C with 100 W microwave power (*Combined*). The indicated microwave powers should be understood as average powers, where 1000 W pulses were distributed over time, namely by pulse-width modulation. The duration of these pulses was approximately 12 s for microwave baking and 4 s for combined baking. Baking conditions for convection and combined baking were chosen based on a series of core temperature measurements during baking using optical fiber temperature probes (FISO), aiming a core temperature between 96 °C and 98 °C. The time for reaching core temperature was weighed against other parameters such as achieving comparable crust formation and coloring of bread, as well as built-in oven features in terms of possible settings for temperature and microwave power. The microwave baking settings were similarly based on core temperature measurements (96–98 °C core temperature). The overall ambition was to choose baking conditions that illustrate possible savings in baking time for different baking techniques. It should be emphasized that the chosen settings are a trade-off and could have been chosen differently. The flours and baking conditions are summarized in Table 1, together with the vertical position of the tomographic volume-of-interest (VOI) from the base of the sample holder. The latter were equal to 1.0 cm, 2.6 cm or 4.1 cm, respectively referred as *Bottom*, *Middle*, and *Top* positions, as illustrated in Fig. 2a.

2.3. Image acquisition

Once the oven had reached a stable baking temperature, the dough was mounted on the sample holder in the oven. Since the safety search of the control hutch at the beamline took between 30 and 60 s, the timer function of the oven was used to delay the start of the microwave heating so that the tomographic imaging could be started prior. X-ray

projection images of the bread were acquired while the sample holder rotated around a vertical axis. The incident near-parallel X-ray beam was a broad band white beam filtered to 50% of power with an energy distributed between 15 and 45 keV and further attenuated by a glass slide to avoid beam damage. The X-rays passing through the bread were converted to visible light by a LuAG:Ce 300 μ m thick crystal scintillator placed 250 mm from the sample, which was subsequently recorded by a custom-made CMOS detector (GigaFROST camera, Mokso et al., 2017). The setup is shown in Fig. 1a. Five hundred radiographic projections covering 180° were acquired per tomogram, resulting in a total scan time of 0.4 s. The image reconstruction was done using a Fourier based re-gridding method (Marone & Stampanoni, 2012). The resulting images captured a bread volume of $5.5 \times 15.3 \times 15.3$ mm³, with a 11 μ m voxel size. A tomogram was acquired every 2.8 s for the microwave series and every 6.4 s for the convection and combined series (except 12.4 s in one series, *Spring wheat-Combined-Middle*). These time-series contained between 50 and 115 reconstructed volumes. In total, 70 bread samples were imaged. Based on various qualitative observations relevant for describing the bread properties, a selection of 30 time series were kept for further analysis. The breads with a cracked crust and deformed shape after baking were discarded. The horizontal slice movies were then inspected and only the series without reconstruction artifacts were kept. At the *Top* position the bread was in some cases evolving too fast compared to the acquisition speed resulting in motion artifacts. This summed up to 1530 volumes.

2.4. Image processing and analysis

The bread image processing consisted of two parts: (1) an image post-processing step, including filtering steps, followed by (2) the image analysis and quantification steps, where several relevant quantitative bread properties, such as porosity, pore size, elongation, local wall thickness and connectivity were extracted (Laverse et al., 2012). First, the gray-level background was homogenized using a top-hat filter (van der Walt et al., 2014). The solid regions were then segmented from the

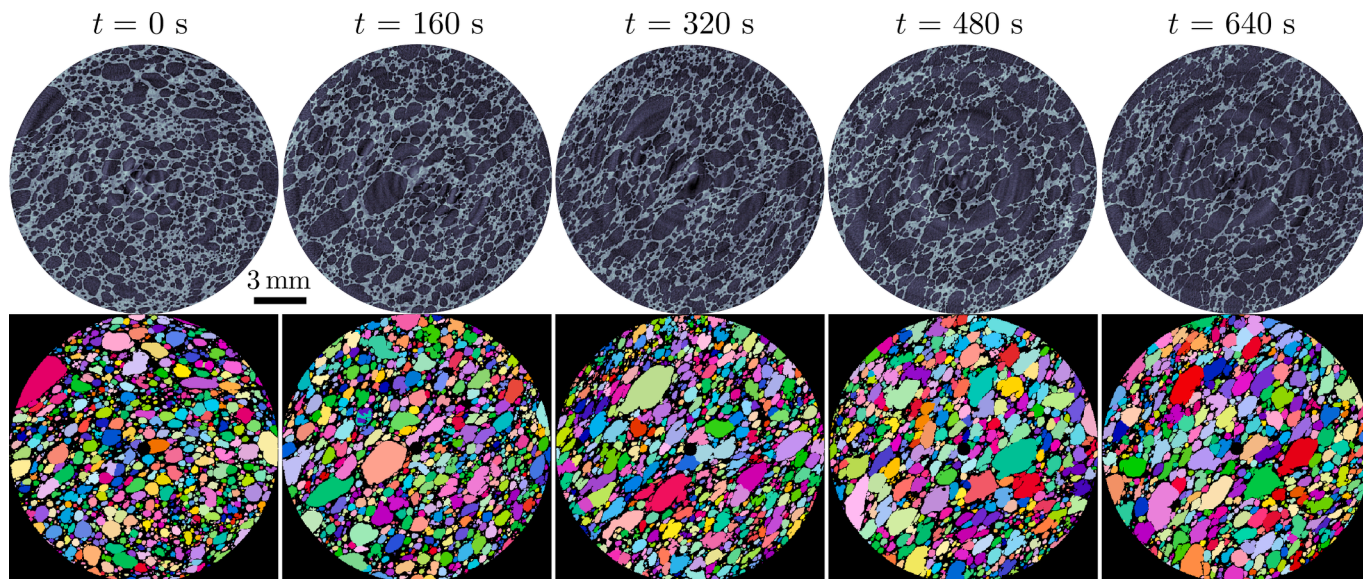


Fig. 4. Horizontal cross-section of reconstructed images (upper row, such as in Fig. 3b) in the middle of the 3D volume, and corresponding pore-separated images (lower row, such as in Fig. 2d) at different times during baking of an Extra-Convective-Middle series. The bread lamellar structures appear brighter, and the air pores appear darker in the upper row. The pores are labelled with arbitrary colors in the lower row.

pore space using the Otsu's thresholding method (van der Walt et al., 2014). The individual pores were identified from these binarized images using the ITK watershed algorithm (Stamati et al., 2020). Ring artifacts were observed in the reconstructed images close to the center of rotation (Barrett & Keat, 2004). Therefore, a central cylindrical mask was applied along the axis of rotation (0.25 mm radius). The pore regions being cut at the top and bottom of the volume and at the edge by the cylindrical mask were removed to prevent bias in the calculated properties. As an illustration, the post-processing steps for the first volume (at baking time $t = 0$ s), from the *Extra-Convective-Middle* series are shown in Fig. 2: (b) reconstructed volume of interest image, (c) segmented image, (d) separated pores and (e) separated pores with removed pores at the edges. There were typically between 1000 and 10,000 pores per image.

The different image analysis measures determined in this work are shown in Fig. 3. The porosity and local wall thickness were extracted from the binarized images (Fig. 2c). The pore volumes, elongations and coordination numbers were extracted from the separated pores, with removed pores at the edges (Fig. 2e). Porosity ϕ_g was defined as the number of void voxels divided by the total number of voxels in the image, i.e., with n_g gas and n_s solid voxels, $\phi_g = \frac{n_g}{n_g + n_s}$. Local wall thickness h_w was extracted using the fast local thickness algorithm developed by Dahl and Dahl (2023). In Fig. 3, on the left-hand side, a local wall thickness sub-volume is shown. The colors indicate the measured local thicknesses. The larger local-wall thicknesses are shown in red and the smaller ones in dark blue. The mean local wall thickness $\langle v \rangle$ is the average of the non-zero local-wall thickness values in the image. In the same figure, on the right-hand side, a separated pore sub-volume is shown. The pores are labelled with arbitrary colors. The pore volume was computed as the number of voxels in each pore region. Given the set of coordinate of a pore $\{r\}$, its center of mass position is $\langle r \rangle_j$, then its shape tensor can be defined as $S = \langle (r - \langle r \rangle_j) \otimes (r - \langle r \rangle_j) \rangle_j^{1/2}$, here with $\langle \dots \rangle_j$ the average over all voxels j (Raufaste, Dollet, Mader, Santucci, & Mokso, 2015). The elongation E of each individual pore was based on the principal components as the ratio of the maximum shape eigenvalue (S_{max} , the major semi-axis) by the minimum shape eigenvalue (S_{min} , the minor semi-axis): $E = S_{max}/S_{min}$. The elongation is by construction greater or equal to 1. As an example, the elongation of a pore (in cyan color) is shown in Fig. 3. The coordination number Z was defined as the number of touching neighbors in the separated pore

image. It can also be seen as the number of open contacts between a pore and its neighboring pores, or the connectivity between neighboring pores. It was directly extracted by the function 'labelledContacts' available in the SPAM python package (Stamati et al., 2020). As an example, the coordination number of one pore (in mustard color) is shown in Fig. 3. The mean pore volume $\langle V \rangle$, mean elongation $\langle E \rangle$ and mean coordination number $\langle Z \rangle$ were computed as an average value over all pores in an image. For more details, an example of batchwise quantification is showed as a jupyter notebook in foamquant documentation (Foamquant documentation, 2023).

To evaluate the accuracy of the method we do the following consideration. The main source of error originates from the image segmentation due to the finite resolution of 2–3 voxels in the 3D reconstructions. The mean pore volume in the imaged bread samples ranged between 13,500 and 45,000 voxels. A segmentation uncertainty of 1 voxel would lead to a possible inaccuracy on the pore size measurement of 0.8–2.0 %.

3. Results and discussion

3.1. Structure evolution during baking

The concept developed in this work makes it possible to monitor the three-dimensional structure evolution *in-situ* during the transformation from dough to bread and to determine quantitative parameters of the bread structure during the baking. One example of such a structure evolution is shown in Fig. 4. The horizontal cross-section of reconstructed images (upper row) in the middle of the 3D volume, and corresponding pore-separated (lower row) of an *Extra-Convective-Middle* sample are shown at different times during baking. The bread structure starts typically at a low porosity, with small, isolated, and slightly elongated pores. During baking, the microstructure evolves with an increasing porosity, decreasing local wall thickness, and an increasing mean pore volume, elongation, and coordination.

SRμCT provides full 3D information about the structure evolution and consequently distributions of all measured quantities. Distribution representation allows quantitative comparison between the series while preserving the richness and complexity of the extracted data. The quantified individual pore volume V , coordination number Z , elongation E , and local wall thickness h_w showed significant spread inside each

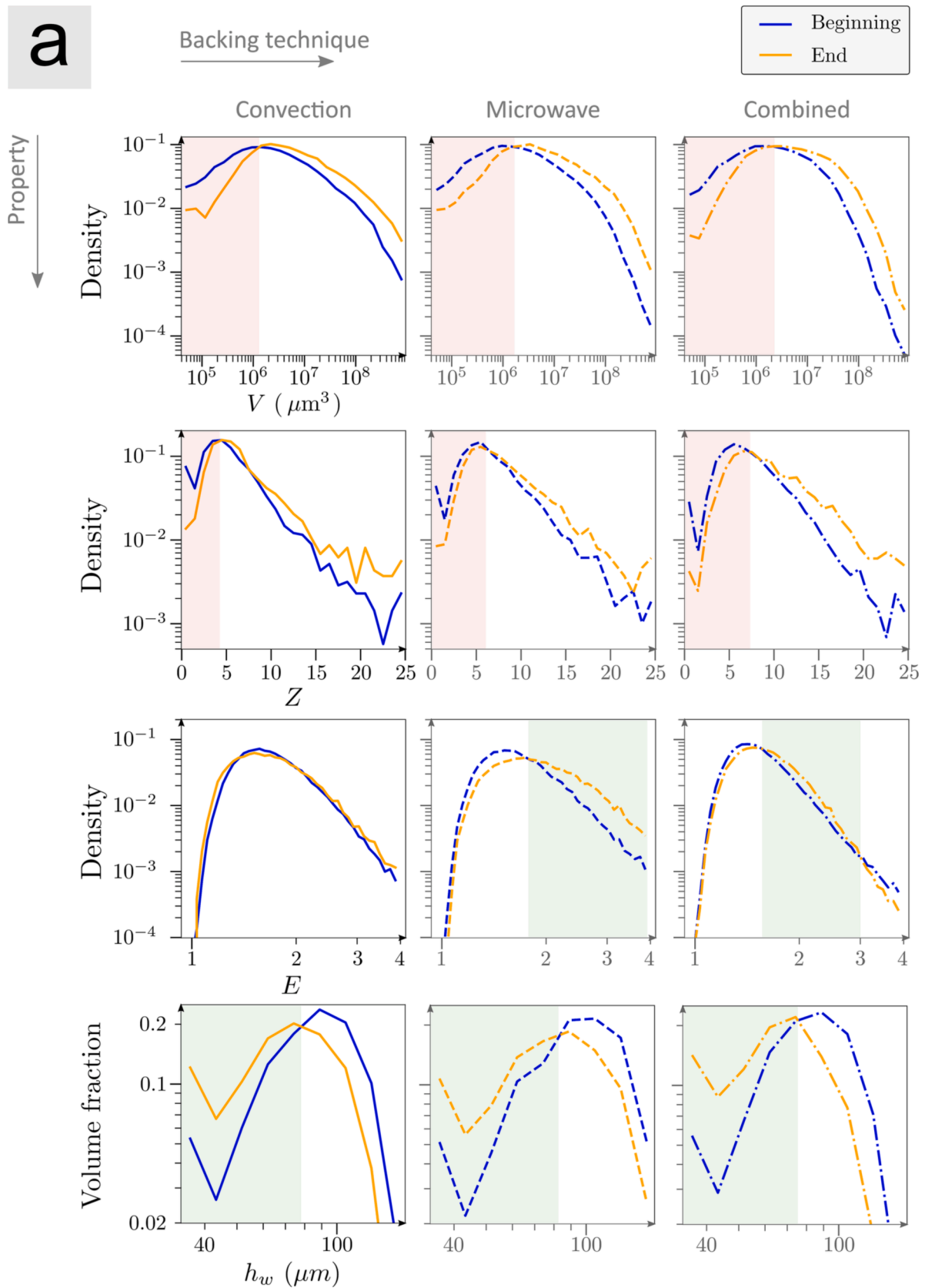


Fig. 5. (a) Density distributions of the pore volume V , coordination Z , elongation E , and volume fraction of local-wall thickness h_w (normalized by the solid fraction), at the beginning and end of the baking, for the Extra-Middle samples with different baking technologies. For recall, see their definition in [section 2.4](#). The orange line is the distribution in the beginning (proofed state) and the blue line is the distribution in the end (final state). The red backgrounds emphasize the ranges for which the final distribution is below the initial one, and the green backgrounds emphasize the ranges for which the final distribution is above the initial one. (b) Corresponding frequency distributions of pore volume V , coordination Z and elongation E , as well as local-wall thickness h_w as a function of time. The frequency is shown by the

color level and is logarithmically scaled. Blue indicates a low frequency and red indicates a high frequency. If the frequency is equal to zero, the pixel is shown in white. The white vertical bands for Microwave and Combined, are a consequence of microwave-pulse-induced motion artifacts – those images were excluded from the analysis. The arrow symbols (\blacktriangleright) show the loss of the non-connected pores during baking. The oval symbols (\bullet) show the simultaneous decrease in elongation and number of pores in the volume-of-interest. The diamond symbols (\blacklozenge) show structure relaxations after microwave pulses. (For interpretation of the references to color in this figure legend, the reader is referred to the web version of this article.)

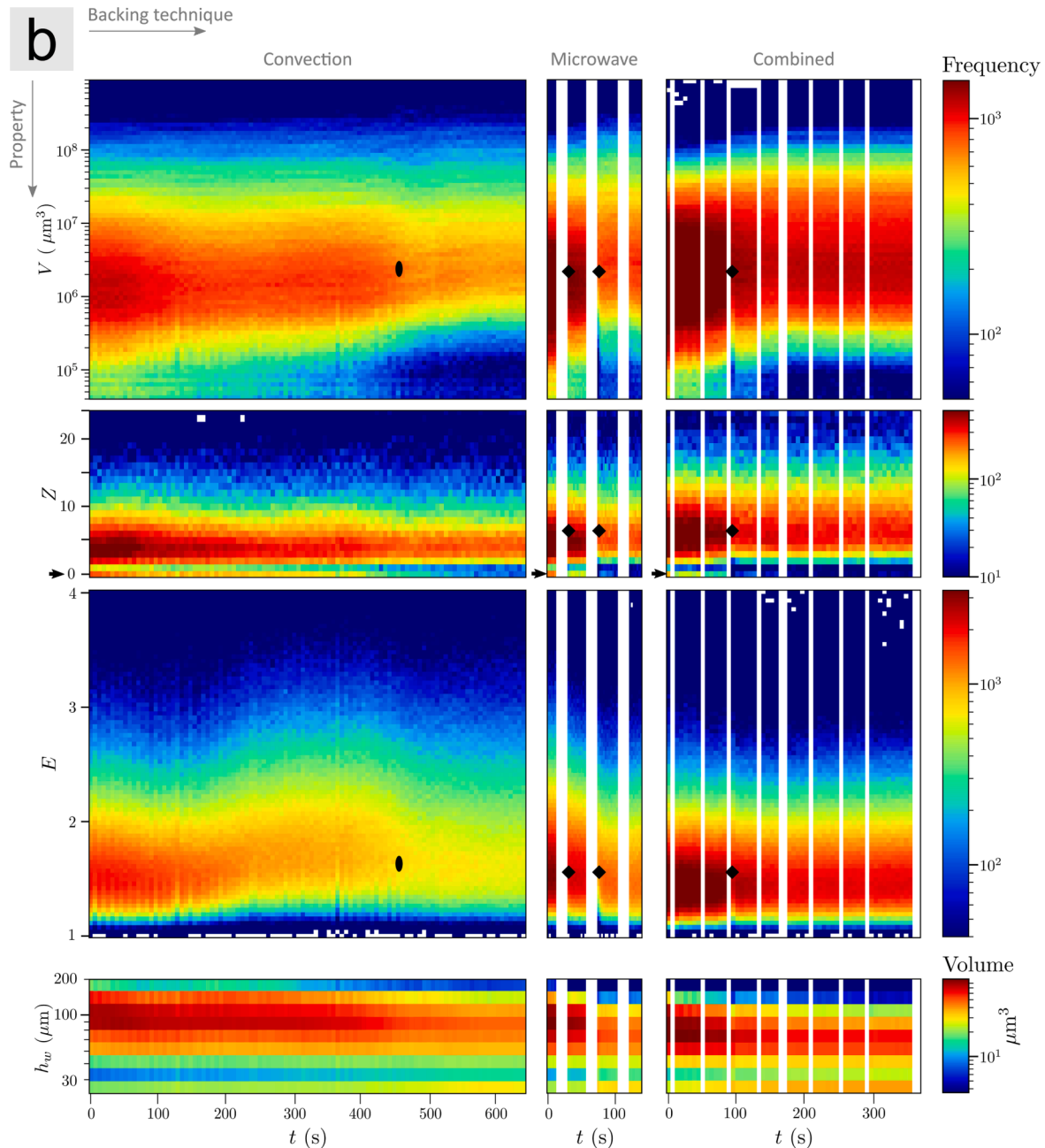


Fig. 5. (continued).

single image. Density distributions of the individual pore volume V , coordination number Z , elongation E , and local wall thickness h_w for Extra-Middle and Convection, Microwave and Combined are shown in Fig. 5. The distributions at the beginning and end of the baking are shown in blue and orange in Fig. 5a. The corresponding time resolved frequency distributions are shown in Fig. 5b.

The density distribution evolutions are quite similar between the three different baking techniques in Fig. 5a. The number of pores typically decrease inside the VOI, while the distribution profiles only change slightly during baking supporting the importance of proofing on the final baked state (Fig. 5a). More differences during baking can however be

observed in Fig. 5b.

First of all and as expected, the evolutions for Convection is slow and continuous while for the two other baking techniques, changes occur stepwise due to the microwave pulses. The volume density distributions before and after baking typically show a peak around $1 \cdot 10^6$ – $2 \cdot 10^6 \mu\text{m}^3$ (0.001 – 0.002 mm^3). In the end, the distribution is not only simply shifted to larger volumes. The number of small pores decreases, and the number of large pores increases. The orange curves flatten at the smallest volumes, indicating a preservation of a few smallest pores through baking for the three baking techniques (below $1 \cdot 10^5 \mu\text{m}^3$). The coordination distribution provides information about the connectivity

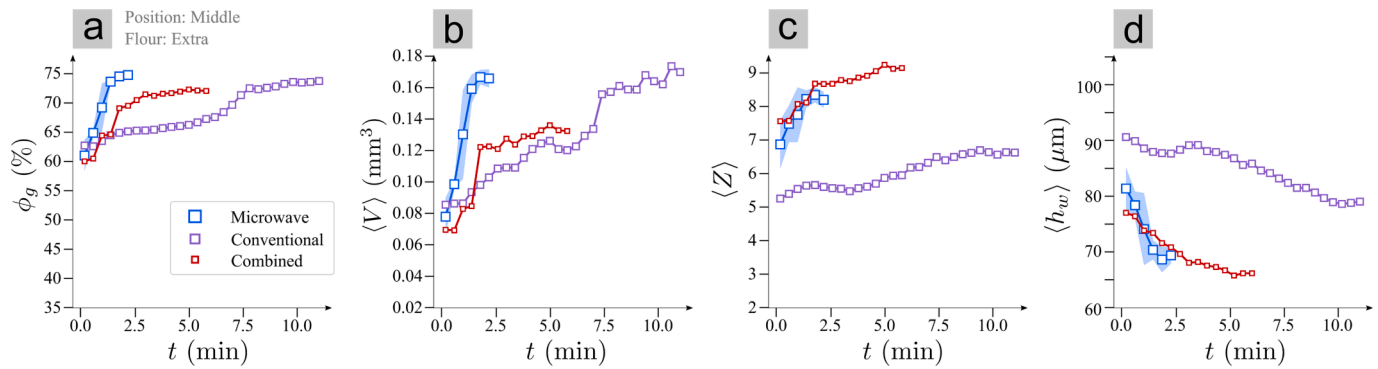


Fig. 6. Effect of baking technologies (Microwave, Conventional and Combined). Time-averaged porosity ϕ_g , mean pore volume $\langle V \rangle$, mean pore coordination $\langle Z \rangle$, and mean local wall thickness $\langle h_w \rangle$ as a function of time for Extra-middle (a–d). For recall on the quantifications see their definition in Section 2.4. The standard deviation between the Microwave series is indicated as a shaded area around the mean values (2 replicates). Only one Extra-Middle sample was imaged with Conventional and Combined baking.

between pores. In general, the connectivity increases with time and the highly connected pores become relatively more numerous with time. There are initially more non-connected pores ($Z = 0$) than pores connected with one other pore ($Z = 1$), but this difference tends to decrease during baking. See the bottom non-connected line in Fig. 5b (► symbols). At all times, larger pores were more connected, but without any dependency on their elongation (not shown here). The walls around small and more isolated pores are breaking. These pores subsequently merge with larger and already more connected pores.

The elongation distributions for Convection at the beginning and at the end were nearly identical, see Fig. 5a. The pores elongated above 1.3 become relatively more numerous for Microwave as indicated with green background in Fig. 5b. The same trend as for Microwave can be seen also for Combined, but the trend is weaker. Often during Convection baking and for the different flours, a 2 to 3 min long jump in elongation is observed, with an increased spread of the values (such as shown in Fig. 5b, Convection). Here during the jump, the elongation increases approximately by 0.5. Then, the pores relax and become less elongated simultaneously with a sudden decrease in the number of pores in the VOI (decreasing frequency in Fig. 5b, ◊ symbols). These jumps were not observed with Microwave nor Combined heating. One possible explanation for this behavior can be attributed to the heat fronts propagating through the breads during Convection baking. Elongation was also temporarily increased by the microwave pulses. Within 20–30 s, the structure relaxes with a decreasing elongation (◊ symbols in Fig. 5b, elongation subfigures). These fast evolutions can sometimes be seen at the same times for V and Z (◊ symbols) with temporarily slightly larger and more connected pores. The local wall thickness distribution shows

typically an increase of volume fraction in the small walls (below 70 – 80 μm, green background). Due to the space resolution limitation, the wall thickness points below 33 μm are cumulated measures of the thicknesses below 33 μm (Fig. 5a), and the large number of the smallest walls are explained by the cumulation.

3.2. Comparison of the baking processes

The influence of the baking technologies (Microwave, Conventional and Combined) on the porosity ϕ_g , mean pore volume $\langle V \rangle$, mean pore coordination $\langle Z \rangle$, and mean wall thickness $\langle h_w \rangle$ is shown as a function of time for the Extra-Middle series in Fig. 6a–d. Although they are not all starting exactly at the same levels, for the different properties, due to natural variations in proofing, clear differences in structure evolution can be observed. As expected, microwave-baking immediately heat the core of the buns, which accelerate the baking process. The ready-baked state is reached first by Microwave, followed by Combined and finally by Convection. A plateau in porosity and pore mean volume is reached after about 8 min for Convection, while after approximately 1.5 and 2.5 min for Microwave and Combined, respectively, see Fig. 6a and b. The porosity and mean volume follow an S-shaped increase as a function of time for all the three baking technologies. This S-shaped evolution may be interpreted as the so-called “oven spring” describing the stage where the maximum rise of the bread occurs due to steam and carbon dioxide expansion, resulting in a non-linear increase in pore volume (Zhang, Datta, & Mukherjee, 2005). Note an accelerated increase in porosity and mean pore volume after approximately 7.5 min for Convection, which is absent for microwave heating. This increase can be compared with the

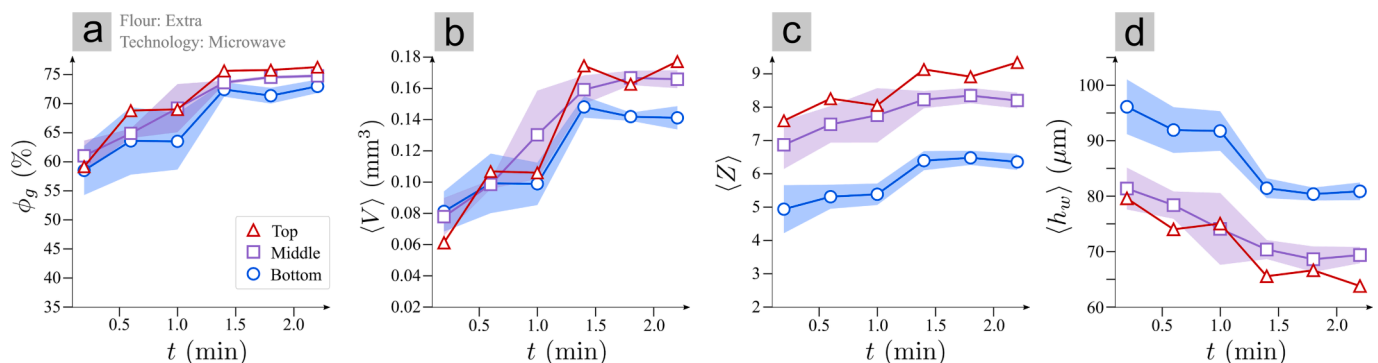


Fig. 7. Effect of the vertical position (Top, Middle and Bottom) inside the breads). Time-averaged porosity ϕ_g , mean pore volume $\langle V \rangle$, mean pore coordination $\langle Z \rangle$, and mean local wall thickness $\langle h_w \rangle$ as a function of time for Microwave-Extra (A–D). For recall on the quantifications see their definition in Section 2.4. The standard deviation between the series is indicated as a shaded area around the mean values (2 replicates for Middle and 2 for Bottom). Only one sample was imaged at the Top position.

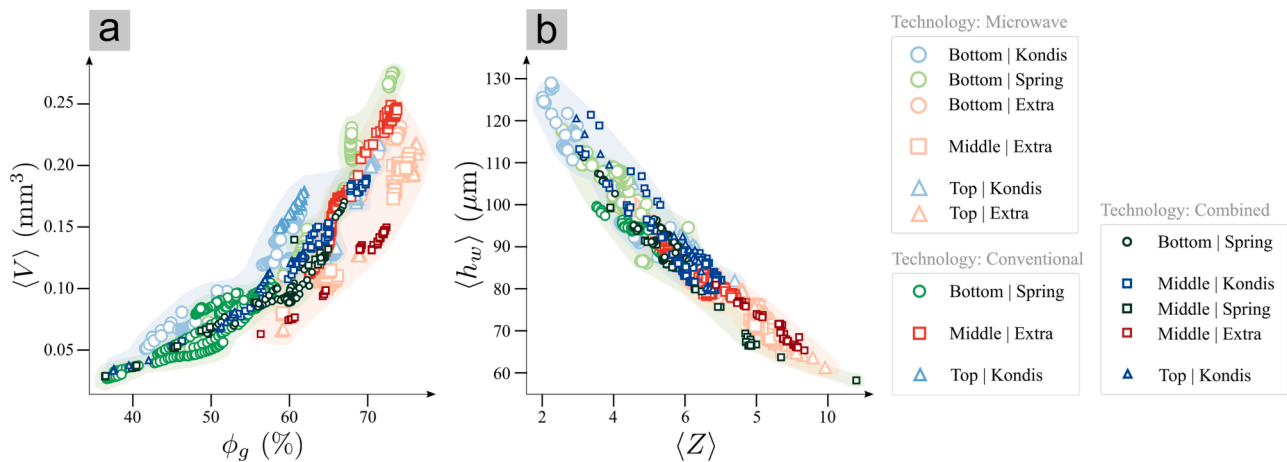


Fig. 8. Correlations between measured structure properties, defined in Section 2.4. (a) Mean pore volume $\langle V \rangle$ as a function of the porosity ϕ_g . (b) Mean local thickness $\langle h_w \rangle$ as a function of the mean coordination number $\langle Z \rangle$ of all the series. Each point corresponds to an analyzed image (1530 points in total). The flour type clusters were drawn in background light colors for eye-guide (green for Spring wheat, Blue for Kondis and red for Extra). (For interpretation of the references to color in this figure legend, the reader is referred to the web version of this article.)

shift in elongation observed in Fig. 5b (● symbols). It is primarily attributed to the heat front propagation through the bread. This difference between microwave and conventional baking with regard to heat propagation from the exterior to the interior have been well described and are summarized in the reviews by Gülüm (2001) and Bon-Orm, Jury, Boillereaux, and Le-Bail (2023). In addition, similar differences in porosity depending on the baking technology have also been observed by Datta et al. (2006), using various analytical *non-in-situ* techniques. Fig. 6c, shows increasing mean coordination number and decreasing mean wall thickness with time for the three technologies. The lamellas slowly become in average thinner and thinner, and more and more of them break between the pores, which agrees with previous findings (Nicolas, Glouannec, Ploteau, Salagnac, & Jury, 2017). Convection shows a slight decrease in mean coordination (0.5 in average) and increase in mean wall thickness around 2 min (Fig. 6c and d), which corresponds to a plateau in porosity (Fig. 6a). This reason for this can be that when the ratio between air and material in the bun (the porosity) stops increasing, although the mean pore size stills increase, the cell wall thickness must also decrease.

3.3. Baking homogeneity – The effect of position in the bread

The effect of the vertical position in the bread (*Top*, *Middle* and *Bottom*) on the porosity ϕ_g , mean pore volume $\langle V \rangle$, mean pore coordination $\langle Z \rangle$, and mean wall thickness $\langle h_w \rangle$ is shown as a function of time for the *Microwave-Extra* series in Fig. 7a–d. The evolution of the porosity ϕ_g are similar for the three positions, increasing from around 60% to a plateau at 75% (Fig. 7a). The mean pore volume $\langle V \rangle$ also increases similarly for the three positions, but with a slightly higher pore volume plateau reached for *Top* and *Middle* compared to *Bottom* (around 0.01–0.02 mm³ more, Fig. 7b). The mean coordination number $\langle Z \rangle$ increases with approximately 1.5 for all three positions (Fig. 7c). The mean local wall thickness $\langle h_w \rangle$ decreases with about 15 μm for the three positions (Fig. 7d). The final states for $\langle Z \rangle$ and $\langle h_w \rangle$ are clearly influenced by the initial proofing, with a lower average number of open walls and thicker lamellas at the *Bottom* (2.5–3 less open walls and 15 μm thicker than at the *Top*). More information about initial proofing can be found in appendix B. In the *Bottom*, the slightly smaller porosity, mean pore volume, smaller coordination number and larger mean cell wall thickness are influenced by the crust formation and structure collapse at the bottom of the bun. Microwaves is known to homogeneously heat the bread while convective heat presents a propagation front from the outside. In future studies, this type of analysis could be used to

investigate the microstructure differences induced by these different heat propagations.

3.4. General correlations between structure properties

Correlations between the various microstructure measures have been investigated for all images and experiments included in this study. Two strong correlations have been identified: between the porosity ϕ_g and mean pore volume $\langle V \rangle$, and the mean local wall thickness $\langle h_w \rangle$ and mean coordination number $\langle Z \rangle$, shown in Fig. 8a and b, respectively. Each point corresponds to one analyzed 3D structure. In total, 1530 3D volumes have been examined. For all time-series and during the whole baking process, the mean pore volume increases with increasing porosity, and the mean wall thickness decreases with increasing mean coordination number.

It is interesting to qualitatively investigate how the structures distributes according to baking technology and flour type in Fig. 8a and b. For *Microwave* heating, the points are generally more dispersed in both Fig. 8a and 8b. The points corresponding to *combined* baking is somewhat displaced towards low porosity and low mean pore volume, whereas *conventional* baking is to some extent displaced towards high porosity and high mean pore volume, in Fig. 8a. In Fig. 8b, the points belonging to *conventional* baking is rather centered, whereas the points associated with *combined* baking are nearly as spread as the *microwave* baking points. The data in Fig. 8a and b indicate a dependence between porosity, pore volume and baking technology. But the dependence is much weaker than found in previous studies that showed significant different pore-size distribution depending on the baking technology (Datta, Sahin, Gülüm, & Ozge, 2007). Thus, more research is needed to investigate the relationship between baking technology and evolution of porosity and mean pore volume and to reveal the underlying mechanisms.

A clearer differentiation can however be made between the three flour types (*Spring wheat*, *Kondis* and *Extra*). In Fig. 8a, the points corresponding to the *Spring wheat* flour (green) are in the middle, the *Kondis* points (blue) are slightly shifted to the left and the *Extra* points (red) are slightly shifted to the right. For a given porosity value, the pores in *Kondis* are estimated to be in average around 5% larger and in *Extra* around 5% smaller compared to the *Spring wheat*. The addition of gluten had a significant effect on the structure, with larger porosities reached by *Extra* compared to *Kondis*. It is well known that the final volume of a bread increases linearly with the protein content (Tronsmo et al, 2003). Dough viscoelasticity is directly controlled by the amount of gluten, due to their high non-cross-linked entanglement (He & Hoseneay, 1992). He

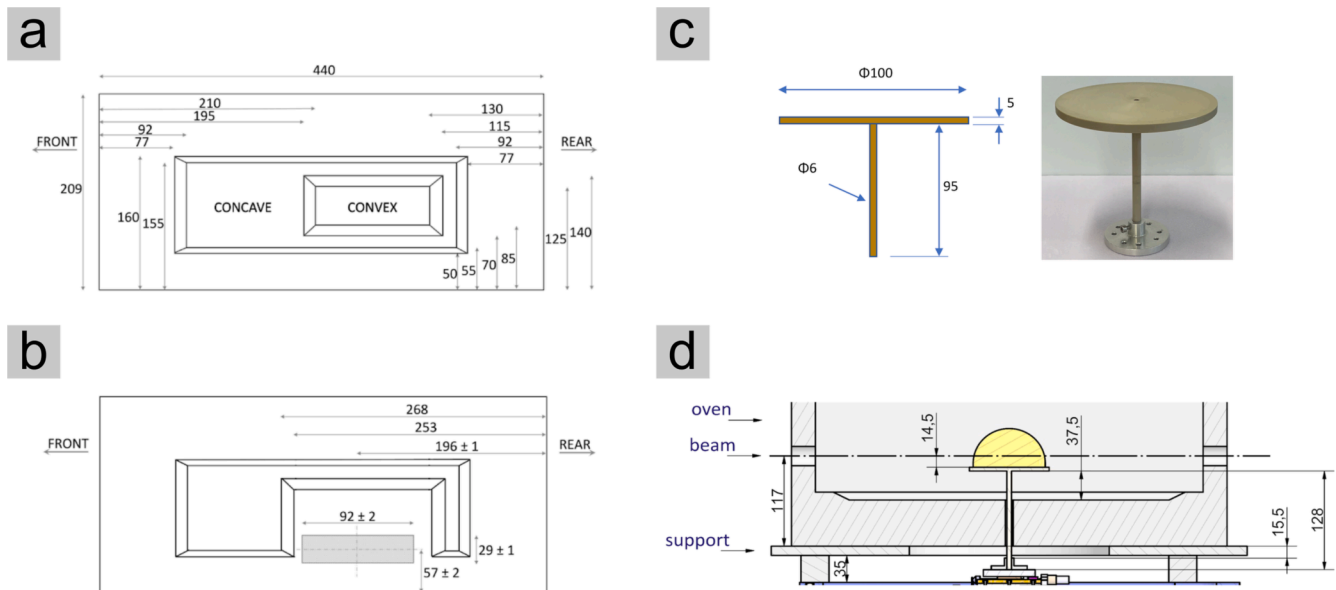


Fig. A1. (a) Location and geometry of press-stamped dents on the left oven's wall before modification (view from the inside of the oven). The front of the oven chamber is on the left (FRONT) and the back is on the right (REAR). The larger dent is concave and the smaller is convex. (b) The resulting dented geometry after modification with the aluminum window shown in filled grey. In (B), only the modification dimensions are indicated. Drawings are not scaled along the vertical and horizontal axis. (c) Dimensions and picture of the PEEK table with the metallic bottom extension. (d) Vertical position of the X-ray beam with the oven and PEEK sample holder.

and Hosenev showed that in dough with lower percentage of protein the cell walls reached their expansion limit before the starch gelatinize, resulting in mechanical failure of the cell wall and the loss of gas. *Kondis* results in a low protein quantity dough, with large starch content and high elasticity. The structure cannot be extended as much as *Spring wheat* and tends to collapse more easily. In *Extra*, when increasing the gluten content, the proportion of filler becomes lower in comparison to gluten, allowing disentanglement of the polymer chains and larger expansion of the dough. However, Tronsmo, Færgestad, Schofield, and Magnus (2003) showed that the final bread volume correlates with the quality of the proteins. The larger porosities reached by *Extra* compared to *Spring wheat* can be attributed to the additional gluten quality difference, being more accessible for reinforcing the bread structure than the naturally present one in *Spring wheat* flour. Here “quality” refers to the combined effect of the proteins, glutenin and gliadins subunits composition, and the molecular weight proportion of proteins and glutenin (Tronsmo et al, 2003). Datta et al. (2007) showed a more complex dependence between the median pore diameter and porosity – both measured with non-in-situ methods. In future studies, their concept of “open”, “closed” and “flow-through”, would be interesting to compare with *in-situ* and *non-in-situ* measures.

In Fig. 8b, the local mean wall thickness shows a negative $-8.8 \mu\text{m}/$ contact slope with the mean coordination number. The reason for this correlation is that a structure with larger average local wall thickness is also a structure in which the pores are more isolated from each other, i. e., with a lower coordination number. Greater resistance to deformation is obtained at larger strains, i.e. strain hardening (Tronsmo et al., 2003). Stretching will therefore preferably occur in the thicker regions of the dough because the thinnest regions are the stiffest, allowing for the bubble to increase before rupturing. If a dough has a high strain hardening index, gas cells can expand before rupturing or coalesce with other cells. Although most literature has focused on the stretchability and strain hardening properties of gluten, the possible role of a liquid lamella, containing soluble materials in the flour, to assist the stretching has recently been proposed (Grenier, Rondeau-Mouro, Dedey, Morel, & Lucas, 2021). In the liquid lamella, the starch also has an important role for the stability of the walls, but how starch and gluten interact and how it affects the pore structure formation is not clear (Meerts, Cardinaels,

Oosterlinck, Courtin, & Moldenaers, 2017). It is also interesting to observe in Fig. 8b that *Kondis* points are mainly located in the top-left corner, the *Spring wheat* in the middle and the *Extra* in the bottom-right corner. The low gluten content induces a more closed structure with larger mean local wall thickness than *Spring*. The addition of gluten results in lower mean wall thickness for *Extra*, even more than for *Spring*.

4. Conclusion

A novel combined microwave-convective oven setup at the TOMCAT imaging beamline (Swiss Light Source synchrotron, Paul Scherrer Institute, Switzerland) was developed. This allowed for sub-second high resolution X-ray microtomographic imaging of the 3D bread structure evolution during baking. A workflow for automatic batchwise image processing, segmentation and analysis of tomographic 3D bread structures was established. Porosity, pore volume, coordination number, elongation and local wall thickness were determined as a function of time.

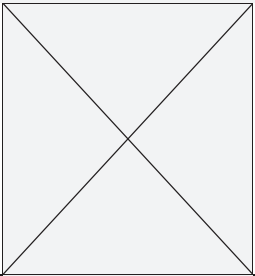
It was possible to obtain high-quality imaging data of the structure evolution both during convective, microwave and combination baking. Microwave baking was the most challenging due to rapid expansion and displacement of the structure.

The results showed that the porosity, mean pore volume and mean coordination number increase with time, and that the mean local cell wall thickness decreases with time. It was found that the evolution of the pores mean elongation was influenced by the heat propagation. Clear dependencies were established between the mean pore volume and porosity, and between the mean local wall thickness and the mean coordination number.

This concept opens new opportunities for the investigation of *in-situ* 3D bread structure evolution, and for development of faster and more energy efficient baking technologies, such as optimized bread baking recipes and improved bread quality and shelf-life. In future work, it will be interesting to follow up on the indication of the weak dependence of the bread microstructure on the baking technique by more careful *in situ* investigations of the structure evolution. It would also be interesting to more carefully investigate the statistical significance of differences due to processing and formulation of the bread. However, that would require

Table B1

Initial proofed state of the breads with three types of flours and at the three positions. The mean value and standard deviation are shown. The mean value is obtained by taking the average of the acceptable samples of the three baking techniques for each specific flour and position. The maximum values, line by line, are shown in bold. The minimum values, line by line, are underlined.

Position	Property	Symbol	Spring wheat	Kondis	Extra
Top	Number of samples		0	3	1
▲	Porosity	ϕ_g (%)		64 ± 15.0	59.2
	Volume	$\langle V \rangle$ (mm ³)		0.063 ± 0.045	0.061
	Coordination	$\langle Z \rangle$ (-)		5.26 ± 1.18	7.59
	Wall thickness	$\langle h_w \rangle$ (μm)		108.6 ± 11.6	79.6
Middle	Number of samples		1	3	5
□	Porosity	ϕ_g (%)	<u>39.0</u>	52.2 ± 3.6	60.6 ± 2.3
	Volume	$\langle V \rangle$ (mm ³)	<u>0.033</u>	0.062 ± 0.007	0.075 ± 0.011
	Coordination	$\langle Z \rangle$ (-)	4.66	<u>4.50 ± 0.58</u>	6.56 ± 0.88
	Wall thickness	$\langle h_w \rangle$ (μm)	93.8	104.4 ± 9.6	<u>83.1 ± 5.6</u>
Bottom	Number of samples		8	2	2
○	Porosity	ϕ_g (%)	46.6 ± 5.0	<u>42.8 ± 1.6</u>	58.5 ± 4.2
	Volume	$\langle V \rangle$ (mm ³)	0.046 ± 0.011	<u>0.041 ± 0.004</u>	0.081 ± 0.013
	Coordination	$\langle Z \rangle$ (-)	3.59 ± 0.75	<u>2.39 ± 0.36</u>	4.94 ± 0.72
	Wall thickness	$\langle h_w \rangle$ (μm)	107.0 ± 7.2	122.6 ± 4.8	<u>79.6 ± 4.2</u>

a larger number of replicates, a more comprehensive experimental design and more beamtime.

Funding Information

This work was funded by VINNOVA (Sweden's Innovation Agency) [2019–02572], and additional internal RISE co-financing from 2020. Florian and Rajmund were financed by the Swedish Research Council [2019–03742]. Niklas gratefully acknowledges funding from the Swedish Research Council [2018–06378]. The computations and data handling were carried out under the following QIM-related projects: SNIC 2022/6–157 and LU 2022/2–22, which were enabled by resources provided by the Swedish National Infrastructure for Computing (SNIC) at LUNARC at Lund University, partially funded by the Swedish Research Council through grant agreement [2018–05973].

Declaration of Competing Interest

The authors declare that they have no known competing financial interests or personal relationships that could have appeared to influence the work reported in this paper.

Data availability

Data will be made available on request.

Acknowledgements

We acknowledge the Paul Scherrer Institut, Villigen, Switzerland for provision of synchrotron radiation beamtime at beamline TOMCAT of the SLS and would like to thank Gordan Mikuljan and Christian Matthias Schlepütz for technical support. Lars Jennergren, Abdon Foods (Finax Bröd) is acknowledged for materials and valuable input on the design of the project. We would like to thank Electrolux for providing the study with two ovens, and thank Tomas Rydholm, RISE, for choosing the oven model, helping with oven design, and arranging reception of ovens at RISE. Moa Thorén, Chalmers, who did a pre-study as her master thesis to study the impact of gluten content and baking technology on volume and crumb formation in wheat bread is acknowledged.

Appendix

A. Oven modifications

The dimensions of the oven chamber given by the manufacturer documentation are shown in Fig. A.1a. The oven had walls which met the ceiling, the back, and the floor of the chamber in a curved way. The positions of the modified windows were measured from where the

curvature ends. The holes were cut in the metal casing and in the mineral wool insulation-layer, with the approximate size and positions illustrated in Fig. A.1b in grey. The flat-field measurements were done without bread on the sample holder. At the Tomcat beamline, the oven and PEEK sample holder (Fig. A.1c) were positioned in such a manner that the beam would pass 117 mm above the support on which the oven rested (Fig. A.1c). With the sample holder in its lowest position, this allows a free passage of the beam for any bread with a height below 52 mm ($37.5 + 14.5$), as shown in Fig. A.1d.

B. Proofed dough structure

The proofed dough structure is the state from which the bread evolves through baking. The proofed strongly influences the resulting baked state. The proofing conditions (proofing time and temperature) were kept constant in our experiments regardless of the flour type. This resulted in variation between the flour types and positions in the imaged bread. It is well known that flour strength, protein content and absorption of water affect fermentation time and volume (Zghal, Scanlon, & Sapirstein, 2001). Weak low-protein flours rise faster during proofing and flours with a high protein content usually form bread with a higher volume than low-protein flours (He & Hoseney, 1992). Measured porosity, mean pore volume, mean pore coordination number, and mean wall thickness are shown for the different cases in Table B.1 Overall, the porosity varied between 40 and 60%, the mean pore volume between 0.03 and 0.08 mm³, the mean pore coordination between 2 and 8 neighbors, and mean wall thickness between 80 and 120 µm. As expected, different initial states were observed as a function of the flour type and the position inside the bread. The *Extra* and *Kondis-Top* dough structures showed the largest porosity, around 60 %, with a more homogeneous porosity for *Extra* compared to *Kondis*. The *Extra-Middle* and *Bottom* had substantially larger mean pore volume compared to the other cases, and *Extra* had the highest mean coordination number for all positions compared to the other flours. On the other hand, the *Kondis* flour had the largest mean wall thickness for all positions compared to the other flours. The *Extra* proofed structure is more homogeneous over the vertical positions than *Kondis*, with initially smaller porosity, larger and more connected pores, and finer bread lamellas. *Kondis* has a similarly fine structure at the top but gradually gets a coarser structure when going to the middle and bottom positions.

Appendix A. Supplementary material

Supplementary data to this article can be found online at <https://doi.org/10.1016/j.foodres.2023.113283>.

References

- Wäppling Raaholt, B., Wahnström, E., Börjesson, M. (March 2011). Energy efficient baking of bread - measurements on industrial bakery lines, *SIK report, a project in Food Strategy for Sweden Dnr 19-8003/08*.
- Wäppling-Raaholt, B. (Sep 2013). Combined microwave-infrared convective baking of bread, In *Conference proceedings of the AMPERE international conference on MW and HF heating*, Nottingham, UK, pp. 35-39.
- Wäppling Raaholt, B. (March 2015). Energy-efficient baking using alternative technologies: pan bread, string bread and crisp bread, *the Swedish Energy Agency, STEM report*.
- Wäppling Raaholt, B. (Spring 2020). Energy-efficient baking using alternative technologies: crisp rolls and loaves, *the Swedish Energy Agency, STEM report*.
- Mondal, A., & Datta, A. K. (2008). Bread baking - A review. *Journal of Food Engineering*, 86, 465–474. <https://doi.org/10.1016/j.jfoodeng.2007.11.014>
- Chhanwal, N., Tank, A., Raghavarao, K. S. M. S., & Anandharamakrishnan, C. (2012). Computational Fluid Dynamics (CFD) modeling for bread baking process—A review. *Food and Bioprocess Technology*, 5, 1157–1172. <https://doi.org/10.1007/s11947-012-0804-y>
- Briceño-Ahumada, Z., Mikhailovskaya, A., & Staton, J. A. (2022). The role of continuous phase rheology on the stabilization of edible foams: A review. *Physics of Fluids*, 34, Article 031302. <https://doi.org/10.1063/5.0078851>
- Sluimer, P. (2005). Principles of breadmaking: functionality of raw materials and process steps. [WWW Document]. <<https://www.thefreelibrary.com/Principles+of+Breadmaking%3a+Functionality+of+Raw+Materials+and+Process...+a0138810611>> Accessed 10.12.22.
- Primo-Martín, C., van Dalen, G., Meinders, M. B. J., Don, A., Hamer, R. H., & van Vliet, T. (2010). Bread crispness and morphology can be controlled by proving conditions. *Food Research International*, 43, 207–217. <https://doi.org/10.1016/j.foodres.2009.09.030>
- Falcone, P. M., Baiano, A., Conte, A., Mancini, L., Tromba, G., Zanini, F., & Del Nobile, M. A. (2006). Imaging techniques for the study of food microstructure: A review. *Advances in Food and Nutrition Research*. Elsevier, 205–263. [https://doi.org/10.1016/S1043-4526\(06\)51004-6](https://doi.org/10.1016/S1043-4526(06)51004-6)
- Falcone, P. M., Baiano, A., Zanini, F., Mancini, L., Tromba, G., Dreossi, D., Montanari, F., Scuro, N., & Nobile, M. A. D. (2006). Three-dimensional quantitative analysis of bread crumb by X-ray microtomography. *Journal of Food Science*, 70, E265–E272. <https://doi.org/10.1111/j.1365-2621.2005.tb07182.x>
- Lassoued, N., Babin, P., Della Valle, G., Devaux, M.-F., & Réguerre, A.-L. (2007). Granulometry of bread crumb grain: Contributions of 2D and 3D image analysis at different scale. *Food Research International*, 40, 1087–1097. <https://doi.org/10.1016/j.foodres.2007.06.004>
- Laverse, J., Frisullo, P., Conte, A., Del Nobile (2012). X-ray microtomography for food quality analysis, *Food industrial processes - Methods and equipment*. InTech. <<https://doi.org/10.5772/32264>>.
- Babin, P., Della Valle, G., Chiron, H., Cloetens, P., Hoszowska, J., Pernot, P., Réguerre, A. L., Salvo, L., & Dendievel, R. (2006). Fast X-ray tomography analysis of bubble growth and foam setting during breadmaking. *Journal of Cereal Science*, 43, 393–397. <https://doi.org/10.1016/j.jcs.2005.12.002>
- Sun, X., Scanlon, M. G., Guillermic, R.-M., Belev, G. S., Webb, M. A., Aritan, S., Nickerson, M. T., & Koksel, F. (2020). The effects of sodium reduction on the gas phase of bread doughs using synchrotron X-ray microtomography. *Food Research International*, 130, Article 108919. <https://doi.org/10.1016/j.foodres.2019.108919>
- Hu, X., Cheng, L., Hong, Y., Li, Z., Li, C., & Gu, Z. (2021). An extensive review: How starch and gluten impact dough machinability and resultant bread qualities. *Critical Reviews in Food Science and Nutrition*, 1–12. <https://doi.org/10.1080/10408398.2021.1969535>
- Johansson, E., Nilsson, H., Mazhar, H., Skeritt, J., MacRitchie, F., & Svensson, G. (2002). Seasonal effects on storage proteins and gluten strength in four Swedish wheat cultivars. *Journal of the Science of Food and Agriculture*, 82, 1305–1311. <https://doi.org/10.1002/jsfa.1185>
- Chamberlain, N. (1973). Microwave energy in the baking of bread. *Food Trade Review*, 43(9), 8–12.
- Saint-Denis, T., & Goupy, J. (2004). Optimization of a nitrogen analyzer based on the Dumas method. *Analytica Chimica Acta*, 515, 191–198.
- Müller, J. (2017). *Dumas or Kjeldahl for reference analysis? Comparison and considerations for Nitrogen/Protein analysis of food and feed (tech rep.)*. FOSS: Analytics Beyond Measure.
- Thorén, M. (2020). Impact of gluten content and baking method on volume and crumb formation in wheat bread, A pre-study to in-situ 4D synchrotron-based X-ray tomographic analysis of bread during baking. *M. Sc. thesis, Chalmers Univ. of Technology*. <<http://hdl.handle.net/20.500.12380/306489>>.
- Mokso, R., Schlepütz, C. M., Theidel, G., Billich, H., Schmid, E., Celcer, T., Mikuljan, G., Sala, L., Marone, F., Schlumpf, N., & Stamparoni, M. (2017). GigaFRoST: The gigabit fast readout system for tomography. *Journal of Synchrotron Radiation*, 24, 1250–1259. <https://doi.org/10.1107/S1600577517013522>
- Marone, F., & Stamparoni, M. (2012). Regriding reconstruction algorithm for real-time tomographic imaging. *Journal of Synchrotron Radiation*, 19, 1029–1037. <https://doi.org/10.1107/S0909049512032864>
- van der Walt, S., Schönberger, J. L., Nunez-Iglesias, J., Boulogne, F., Warner, J. D., Yager, N., Goullart, E., & Yu, T. (2014). scikit-image: Image processing in Python. *PeerJ*, 2, e453.
- Stamati, O., Andò, E., Roubin, E., Cailletaud, R., Wiebicke, M., Pinzon, G., Couture, C., Hurley, R., Caulk, R., Caillierie, D., Matsushima, T., Bésuelle, P., Bertoni, F., Arnaud, T., Laborin, A., Rorato, R., Sun, Y., Tengattini, A., Okubadejo, O., Colliat, J.-B., Saadatfar, M., Garcia, F., Papazoglou, C., Vego, I., Brisard, S., Dijkstra, J., & Birmpilis, G. (2020). spam: Software for practical analysis of materials. *JOSS*, 5, 2286. <https://doi.org/10.21105/joss.02286>
- Foamquant documentation (2023), <https://foamquant.readthedocs.io>.
- Barrett, J. F., & Keat, N. (2004). Artifacts in CT: Recognition and avoidance. *Radiographics*, 24, 1679–1691. <https://doi.org/10.1148/rg.246405065>
- Dahl, V. A., Dahl, A. B. (2023). Fast local thickness, Proceedings of the IEEE/CVF conference on computer vision and pattern recognition workshops. <<https://github.com/vedranaa/local-thickness.git>>.
- Raufate, C., Dollet, B., Mader, K., Santucci, S., & Mokso, R. (2015). Three-dimensional foam flow resolved by fast X-ray tomographic microscopy. *EPL*, 111, 38004. <https://doi.org/10.1209/0295-5075/111/38004>
- Zhang, J., Datta, A. K., & Mukherjee, S. (2005). Transport processes and large deformation during baking of bread. *AIChE Journal*, 51, 2569–2580. <https://doi.org/10.1002/aic.10518>
- Güllüm, S. (2001). A review on microwave baking of foods. *International Journal of Food Science and Technology*, 36, 117–127. <https://doi.org/10.1046/j.1365-2621.2001.00479.x>
- Bon-Orm, R., Jury, V., Boillereaux, L., & Le-Bail, A. (2023). Microwave baking of bread: A review on the impact of formulation and process on bread quality. *Food reviews international*, 39(2), 1203–1225. <https://doi.org/10.1080/87559129.2021.193129>
- Datta, A. K., Sahin, S., Güllüm, S., & S. Ozge K. (2007). Porous media characterization of breads baked using novel heating modes. *Journal of Food Engineering*, 79, 106–116. <https://doi.org/10.1016/j.jfoodeng.2006.01.046>

- Nicolas, V., Glouannec, P., Ploteau, J.-P., Salagnac, P., & Jury, V. (2017). Experiment and multiphysic simulation of dough baking by convection, infrared radiation and direct conduction. *International Journal of Thermal Sciences*, 115, 65–78. <https://doi.org/10.1016/j.ijthermalsci.2017.01.018>
- Tronsmo, K. M., Færgestad, E. M., Schofield, J. D., & Magnus, E. M. (2003). Wheat protein quality in relation to baking performance evaluated by the Chorleywood bread process and a hearth bread baking test. *Journal of Cereal Science*, 38, 205–215. [https://doi.org/10.1016/S0733-5210\(03\)00027-4](https://doi.org/10.1016/S0733-5210(03)00027-4)
- He, H., & Hoseney, R. C. (1992). Effect of quantity of wheat flour protein on bread loaf volume. *Cereal Chemistry*, 69(1), 17–19.
- Grenier, D., Rondeau-Mouro, C., Dedey, K. B., Morel, M.-H., & Lucas, T. (2021). Gas cell opening in bread dough during baking. *Trends in Food Science & Technology*, 109, 482–498.
- Meerts, M., Cardinaels, R., Oosterlinck, F., Courtin, C. M., & Moldenaers, P. (2017). The impact of water content and mixing time on the linear and non-linear rheology of wheat flour dough. *Food Biophysics*, 12, 151–163.
- Zghal, M. C., Scanlon, M. G., & Sapirstein, H. D. (2001). Effects of flour strength, baking absorption, and processing conditions on the structure and mechanical properties of bread crumb. *Cereal Chemistry Journal*, 78, 1–7. <https://doi.org/10.1094/CCHEM.2001.78.1.1>